

Peter Bächler\*  
Jörg Meyer  
Achim Dittler


# Operating Behavior of Pulse Jet-Cleaned Filters Regarding Energy Demand and Particle Emissions – Part 2: Modeling

Baghouse filters applied for gas cleaning are subject to digitalization concepts, including process modeling and the development of digital twins in order to improve energy efficiency and lower particle emissions. Modeling equations from literature were adapted to match experimental data from part 1 of this study to calculate the effect of varying filter face velocities, dust concentrations, or tank pressures on energy demand and particle emissions. Based on the model approaches, an operation curve that enables the evaluation of filter operation regarding the trade-off between energy demand and particle emissions can be constructed. The identification of energetically optimal cycle times and favorable operation regions is possible due to the extensive experimental framework of the model.

**Keywords:** Energy optimization, Filtration, Particle emission, Process efficiency, Pulse jet-cleaned filters

*Received:* August 31, 2023; *revised:* October 23, 2023; *accepted:* January 16, 2024

**DOI:** 10.1002/ceat.202300409

 This is an open access article under the terms of the Creative Commons Attribution License, which permits use, distribution and reproduction in any medium, provided the original work is properly cited.



Supporting Information  
available online

## 1 Introduction

Baghouse filters are widely applied in industrial gas cleaning processes in order to separate particles from dust-laden gas streams. While in technical applications on the industrial scale stable filter operation is paramount, operation strategies are rarely optimized and the filters are merely a necessity to meet emission standards, protect downstream operation units or enable product recovery. Guidelines such as VDI 3677 offer layout advice for filter houses regarding, e.g., the selection of filter media and the required filter area for certain applications [1].

Nonetheless, baghouse filters are complex systems in which the operation control greatly influences the energy demand and the particle emissions of the facility [2, 3]. During filter operation, particles are primarily separated at the surface of the filter elements, causing increases in cake thickness, flow resistance, and, consequently, differential pressure. Filter regeneration (e.g., via jet pulse) is typically initiated after fixed time intervals ( $\Delta t$ -controlled regeneration) or after exceeding a differential pressure limit ( $\Delta p$ -controlled regeneration) [4]. Typically, not all installed filter elements are regenerated simultaneously; rather, individual bags or individual rows of filter elements are regenerated after meeting the regeneration criterion. Thus, the dust mass deposited on the filter elements is not evenly distributed among all filters and the flow resistance of the different elements may vary greatly. This causes a spatially and temporally variable flow profile through the baghouse filter, where the total volume flow splits depending on the flow resistance of the individual filter elements, resulting in a total

differential pressure between the raw-gas side and the clean-gas side [5, 6]. This behavior is, e.g., not considered in the filter testing standard DIN ISO 11057, where a constant volume flow passes through the filter medium for the entire test procedure and the entire filter area (compared to a subset of the installed filter elements) is regenerated via jet pulse cleaning [7].

The time interval between regeneration events, or the corresponding cake formation, dictates the particle emission behavior. Due to the (almost) perfect separation characteristics of the dust cake, particle penetration through the filter medium is only possible directly after filter regeneration. With sufficient cake formation, the emission quickly declines to a zero level, hence causing an “emission peak” [8]. Longer time intervals between regenerations enable lower average dust emissions at the trade-off of larger differential pressures. Shorter time durations can lower the differential pressure level, where a higher consumption of pressurized air and increased emissions have to be taken into account [2, 9].

In part 1 of this study, experiments were performed in a small-scale baghouse filter with nine filter bags in order to identify feasible operation points regarding the power requirement for filter operation and the corresponding dust emissions [2]. The total power for filter operation was determined as the

---

M.Sc. Peter Bächler (peter.baechler@kit.edu), Dr.-Ing. Jörg Meyer, Prof. Dr.-Ing. habil. Achim Dittler  
Karlsruhe Institute of Technology, Institute of Mechanical Process Engineering and Mechanics, Straße am Forum 8, 76131 Karlsruhe, Germany.

sum of the fan power and the compression energy for the consumption of pressurized air, according to equations shown by Höflinger and Laminger [9]. The optimal cycle times in order to operate at the power minimum were identified for various parameters (filter face velocity, raw-gas concentration, tank pressure). Filter operation at cycle times shorter than the power minimum is not feasible, due to higher dust emissions at no energy benefit. Increasing the cycle time beyond certain limits can significantly increase the differential pressure and the total power, where the benefit of slightly lower particle emissions does not justify the energetic investment. An increase in tank pressure (6 bar vs. 3 bar) for filter regeneration enables a less frequent regeneration (approximately doubled cycle time) at a similar power minimum, with the trade-off of significantly increased dust emissions. Lowering the filter face velocity (or increasing the filter area) can help to lower the overall power consumption of filtration processes. In the context of digitalization, process modeling and the development of digital twins becomes increasingly relevant [10–12].

Modeling of the operating behavior of cleanable filter media ranges back to the mid and late 20th century [13, 14]. An in-depth literature review would exceed the scope of this study and many primary sources were summarized by Löffler [4]. One of the most seminal publications is the work by Leith and Ellenbecker [15]. The total differential pressure across a surface filter medium is typically calculated via the specific resistance of a filter medium  $K_{\text{medium}}$  and the specific resistance of the dust layer  $K_{\text{cake}}$ . The coefficients can be derived from experimental data. However, universal applicability is not guaranteed for every process condition and the coefficients are highly dependent on the type of filter medium and dust [16–18].

A fairly recent noteworthy publication is the work of Klein et al. [19], who presented a calculation tool for the economic optimization of baghouse filters based on model equations. Here, the differential pressure of the filter housing, the dust cake, the filter medium, and the regeneration system including nozzle type and tank pressure were taken into account to identify favorable cycle times regarding the required power for filter operation. The corresponding particle emissions were not taken into account.

In-depth modeling and simulation of the transient separation behavior of surface filters were performed, e.g., by Schmidt and Zhang who focused on cake formation on the micro-scale [20–22]. Full-scale computational fluid dynamics (CFD) simulations to predict the flow and operation behavior of large-scale pulse jet-cleaned filters were presented by Heck and Becker [23].

Part 2 of this study combines the model approach for the layout of surface filters summarized by Löffler [4] and the methodology presented in part 1 of the study [2], which is based on the energy evaluation of filter media presented by Höflinger and Laminger [9].

## 2 Modeling of Filter Operation under Consideration of Energy Consumption and Particle Emissions

### 2.1 Basic Equations for the Layout of Pulse Jet-Cleaned Filters (Ideal Conditions)

While the overall calculation basics for the determination of the differential pressure of a pulse jet-cleaned filter are well documented in the literature (e.g. [4, 24, 25]), the corresponding sources are out of print or difficult to obtain outside of university environments. Thus, this section serves as a repetition of the fundamental equations for the calculation of ideal filter behavior for baghouse filters with multiple filter elements. Assumptions for the calculation include no additional pressure drop due to the housing, homogenous flow conditions, constant process parameters, and an incompressible filter cake. Fig. 1 shows a schematic image illustrating the calculation steps described in this section.

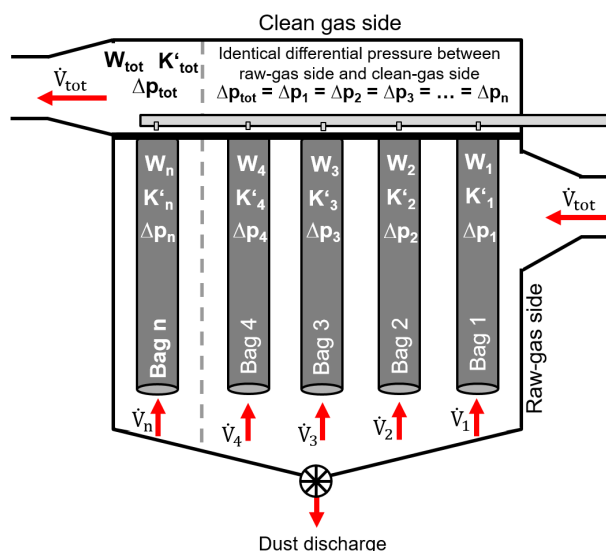


Figure 1. Schematic image of a model filter house with  $n$  filter elements.

The well-known “filter equation” enables the calculation of the differential pressure between the raw-gas side and the clean-gas side across a single filter element  $i$  as a function of the specific filter medium and cake resistances,  $K_{\text{medium}}$  and  $K_{\text{cake}}$ , as well as the deposited dust mass on the filter element  $W_i$  and the filter face velocity  $w_{\text{filter},i}$ .

$$\Delta p_{\text{Filter}} = (K_{\text{medium}} + K_{\text{cake}} \cdot W_i(t)) \cdot w_{\text{filter},i} = (K_{\text{medium}} + K_{\text{cake}} \cdot W_i(t)) \cdot \frac{\dot{V}_i}{A_i} \quad (1)$$

In case of a constant and time-independent filter face velocity (e.g., in case of a single filter element or filter tests with a single circular filter sample – 100% cleaning efficiency), the differential pressure increases linearly (due to typically low filter face velocities) with the deposited dust mass.

The complexity of the calculation increases in case of real baghouse filters with multiple rows of filter elements (Fig. 1). The deposited dust mass  $W_i(t)$  decreases (or in this case is set to zero) due to cake detachment after a regeneration criterion is met. This causes different loading states of the individual filter elements, dependent on the regeneration strategy. Each filter element (or row of filter elements in case of a row-by-row cleaning procedure) has an individual resistance constant  $K'_i$ .

$$K'_i = (K_{\text{medium}} + K_{\text{cake}} \cdot W_i(t)) \quad (2)$$

An overall resistance constant  $K'_{\text{tot}}$  can be calculated for the entire baghouse filter and all filter elements  $n$  (assuming  $A_i = \text{const.}$ ) in order to determine the differential pressure between the raw-gas side and the clean-gas side.

$$K'_{\text{tot}} = \frac{n}{\sum_{i=1}^n \frac{1}{K_i}} \quad (3)$$

$$\Delta p_{\text{Filter}} = K'_{\text{tot}} \cdot w_{\text{filter}} = K'_{\text{tot}} \cdot \frac{\dot{V}_{\text{tot}}}{A_{\text{tot}}} \quad (4)$$

Since the differential pressure between the raw-gas side and the clean-gas side corresponds to the differential pressure across each filter element, the total volume flow  $\dot{V}_{\text{tot}}$  is divided among the filter elements dependent on the flow resistance  $K_i$ .

$$\dot{V}_i = \frac{\Delta p_{\text{Filter}} \cdot A_i}{K_i} \quad (5)$$

The load on the filter elements increases after each time increment  $\Delta t_{\text{increment}}$  according to the raw-gas concentration and the corresponding volume flow through the filter element. This assumes a perfect separation of particles on the filter surface (complete deposition of incoming particle mass on the filter surface). This assumption holds true for most cases of filter operation, where the raw-gas concentrations are in the region of several gram per cubic meter and the emission is (at least) one magnitude lower (maximum emission concentration for fabric filters according to the recent WGC BREF of  $5 \text{ mg m}^{-3}$  for emitted dust mass flows larger than  $50 \text{ g h}^{-1}$  [26]).

$$W_i(t + \Delta t_{\text{increment}}) = W_i(t) + \frac{\dot{V}_i}{A_i} \cdot c_{\text{raw-gas}} \cdot \Delta t_{\text{increment}} \quad (6)$$

Filter regeneration is typically initiated after a preset differential pressure is exceeded ( $\Delta p$ -controlled regeneration) or a time interval has passed ( $\Delta t$ -controlled operation). Here, a  $\Delta t$ -controlled approach was selected similar to the experimental study. After exceeding a cycle time  $\Delta t_{\text{cycle}}$ , the deposited dust mass is reduced to zero. This assumes that the regeneration causes a complete cake detachment of the corresponding filter element.

$$W_i(t) \rightarrow 0 \quad (7)$$

After the determination of the deposited dust mass  $W_i(t)$ , the time is increased by the time increment  $\Delta t_{\text{increment}}$ .

$$t = t + \Delta t_{\text{increment}} \quad (8)$$

This procedure can be repeated for a selected number of time increments in order to model temporally resolved filter

operation. A “steady state” condition is reached relatively quickly so that the average differential pressure for a certain set of parameters does not change significantly. For this study, 20 000 time increments of 1 s each were selected for the creation of each dataset, whereby an average differential pressure for each set of parameters was calculated from the mean of the last 5000 s. An example dataset showing the results for a single set of input parameters can be found in the Supporting Information.

## 2.2 Calculation Parameters for the Validation of the Experiments

The calculation parameters for part 2 of the study were adapted from the previous experiments and are summarized in Tab. 1. Note that these values are mainly relevant for Sect. 3 and the validation of the model from experimental data.

**Table 1.** Calculation parameters.

Parameter	Value
Filter face velocity $w_{\text{filter}}$ [ $\text{cm s}^{-1}$ ]	2, 2.5, and 3.3
Raw-gas concentration $c_{\text{raw-gas}}$ [ $\text{g m}^{-3}$ ]	15 and 30
Cleaning interval $\Delta t_{\text{cycle}}$ [s]	10–180
Number of filter elements $n$ [-]	9
Total filter area [ $\text{m}^2$ ]	4.14
$K_{\text{medium}}$ [ $\text{Pa s m}^{-1}$ ]	10 000–44 000
$K_{\text{cake}}$ [ $\text{Pa m s g}^{-1}$ ]	111

The value for  $K_{\text{cake}}$  could be reliably extracted from uniformly loading the filter elements, starting from a point where all filter elements were recently regenerated without any deposited dust mass ( $W = 0$ ). While  $K_{\text{medium}}$  can be determined in a similar manner (for  $W_i = W_{\text{tot}} = 0 \rightarrow \Delta p = w_{\text{filter}} \times K_{\text{medium}}$ ), the actual medium resistance may vary during filter operation. For example, the regeneration pressure can play a role in the residual pressure drop after filter regeneration due to effects like patchy cleaning [27]. As a result,  $K_{\text{medium}}$  is the main optimization parameter to better describe the experimental data by the model in Sect. 3.1.1.

## 2.3 Consideration of the Energy Consumption of Filter Operation

In order to determine the required power for filter operation, the fan power and the compression energy to compensate for the pressure drop in the pressure vessel due to filter regeneration were calculated. These equations were used by Höflinger and Laminger [9] in order to evaluate filter media based on energy criteria in a past study, as well as in part 1 of this study [2].

$$P_{\text{Filter}} = P_{\text{fan}} + P_{\text{reg}} \quad (9)$$

$$P_{\text{fan}} = \dot{V}_{\text{tot}} \cdot \Delta p_{\text{Filter}} \quad (10)$$

$$P_{\text{reg}} = \frac{V_{\text{tank}} \cdot \Delta p_{\text{tank}}}{\Delta t_{\text{cycle}}} \quad (11)$$

The pressure drop in the vessel  $\Delta p_{\text{tank}}$  was determined experimentally for different regeneration pressures according to part 1 of the study, and the volume of the vessel  $V_{\text{tank}}$  is  $0.011 \text{ m}^3$ .

## 2.4 Modeling of Particle Emissions for Filter Regeneration

The particle emission of pulse jet-cleaned filters follows a distinct behavior. Directly following filter regeneration, particles may penetrate the filter medium. The medium itself is commonly optimized regarding its surface properties (e.g., laminated membrane on the upstream side, singed upstream side, calendered, etc.) to enable a quick formation of a dust cake on the surface. After sufficient cake formation (deposited dust mass on filter element  $W_i(t)$ ), the emission drops to a zero level due to the high separation efficiency of the dust cake.

Löffler [4] offers the following equation according to Valentin for the calculation of the (total) separation efficiency linked to the transient particle emission behavior.  $\kappa$  and  $\delta$  are empirical constants:

$$\eta = 1 - \exp\{-\kappa \cdot W_i(t)^\delta\} \quad (12)$$

The transient particle emission concentration can consecutively be calculated as follows:

$$c_{\text{clean-gas}} = c_{\text{raw-gas}} \cdot (1 - \eta) = c_{\text{raw-gas}} \cdot \exp\{-\kappa \cdot W_i(t)^\delta\} \quad (13)$$

According to this function, there is a fixed amount of particulate matter that is emitted after filter regeneration, provided the area weight increases far enough within a complete filtration cycle for the efficiency to reach values close to unity. If the same filter element is regenerated before the emission drops to zero, cake formation is interrupted and the emission peaks early at the single filter element, causing higher average dust emissions within a filtration cycle and a transient “continuous emission”. The time duration during which particles are emitted and the shape of the emission peak depend strongly on the process conditions and the filter medium [28]. Emission peaks taken from filter tests with, e.g., membrane filter media offer only brief durations of several seconds where an emission can be detected. Higher raw gas concentrations and filter face velocities create a higher dust load on

the filter elements and, thus, a faster increase of  $W_i(t)$  and a sharper decline of the emission peak.

While the experimental data would offer a sufficient dataset to model the transient behavior of the total dust emissions from online measurements, the goal of the study is to model the overall trends presented in part 1 of the investigation. In-depth modeling of the dust emission would exceed the scope of this study. Regarding closer insights, Zhang [22] recently showed experimental data and calculation approaches detailing the transition from depth filtration mechanisms directly after filter regeneration to surface filtration and cake build-up.

Thus, a simpler modeling approach is selected instead to predict the total dust emission and its behavior as a function of the cycle time. The total cumulative emitted dust mass per filter area (EDM) can be calculated from online measurements of the clean-gas particle concentration  $c_{\text{clean-gas}}(t)$  according to Eq. (14).

$$EDM = \int_{t_{\text{start}}}^{t_{\text{end}}} c_{\text{clean-gas}}(t) \cdot \frac{\dot{V}_{\text{tot}}}{A_{\text{tot}}} dt = w_{\text{filter}} \cdot \int_{t_{\text{start}}}^{t_{\text{end}}} c_{\text{clean-gas}}(t) dt \quad (14)$$

Similarly, size-resolved determination of the emitted dust mass is possible by considering the weighted particulate matter concentration  $PM_x$  (Eq. (15)).

$$EDM_{PM_x} = \int_{t_{\text{start}}}^{t_{\text{end}}} PM_x(t) \cdot \frac{\dot{V}_{\text{tot}}}{A_{\text{tot}}} dt = w_{\text{filter}} \cdot \int_{t_{\text{start}}}^{t_{\text{end}}} PM_x(t) dt \quad (15)$$

For the experimental dataset of part 1, the emitted dust mass was calculated from the  $PM_{2.5}$  concentration curves.

$$EDM_{PM_{2.5}} = \int_{t_{\text{start}}}^{t_{\text{end}}} PM_{2.5}(t) \cdot \frac{\dot{V}_{\text{tot}}}{A_{\text{tot}}} dt = w_{\text{filter}} \cdot \int_{t_{\text{start}}}^{t_{\text{end}}} PM_{2.5}(t) dt \quad (16)$$

As previously stated, each regeneration event causes the penetration of a distinct amount of particulate matter. In order to validate this assumption, Fig. 2 shows the cumulative emission

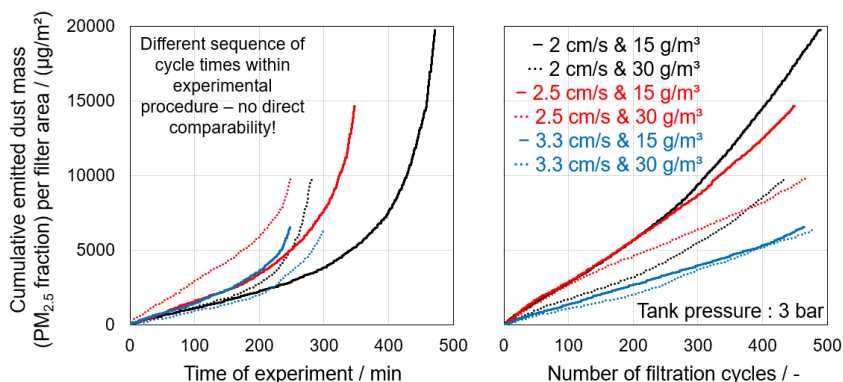


**Figure 2.** Cumulative emitted dust mass of the  $PM_{2.5}$  fraction as a function of the time (left) and the number of filtration cycles (right) for each experiment (compare part 1 of the study) at a tank pressure of 3 bar.

ted particulate matter per filter area ( $EDM_{PM_{2.5}}$ ) over the course of an experimental run for all experiments at 3 bar tank pressure as a function of the time (left) and the number of filtration cycles (right). In part 1 of this study, average  $PM_{2.5}$  concentrations were used as benchmark values to quantify particle emissions due to their health-related relevance and comparability to past studies, where scattered light-based low-cost sensors were used that only have limited output values. Note that, due to the high separation efficiency of pulse jet-cleaned filters, the vast majority of the particle emission is part of the  $PM_{2.5}$  fraction anyway. Emissions at the beginning of an experimental run at a higher cycle time were not considered in the diagram due to higher dust emissions caused by the experimental procedure (compare part 1 of the study). Values at the increased tank pressure of 6 bar can be found in the Supporting Information.

Note that shorter cycle times cause a higher number of filtration cycles in a shorter time duration and therefore a more frequent emission of particulate matter. This leads to a higher slope at the end of the experiment (left diagram), where a state of almost constant regeneration ( $\Delta t_{\text{cycle}} = 10$  s) is reached. When relating the emitted dust mass to the number of filtration cycles instead of the absolute time, the emission increases linearly with increasing number of filtration cycles, validating the assumption of a “fixed” amount of particulate matter being released after each regeneration. Deviations from the linear behavior seem to be prevalent in measurement data with a slower cake formation (e.g., at lower filter face velocities and raw-gas concentrations). Due to the more frequent regenerations, the volume flow passing the recently regenerated filter element is not as high and the flow profile is comparably even. A characteristic  $EDM_{PM_{2.5}}$  value can be extracted from the slope of the diagram (intercept=0). The data for 6 bar tank pressure can be found in the Supporting Information.

In an ideal case, the average emission concentration of the clean gas can be calculated according to Eq. (17). Note that the corresponding clean-gas concentration may also be a weighted  $PM_x$  concentration depending on the used emitted dust mass.

$$c_{\text{clean-gas}} = \frac{EDM \cdot A_{\text{tot}}}{\dot{V}_{\text{tot}} \cdot \Delta t_{\text{cycle}}} = \frac{EDM}{w_{\text{filter}} \cdot \Delta t_{\text{cycle}}} \quad (17)$$

To account for real behavior, an empirical coefficient  $\gamma$  can be introduced to improve the correlation between the measurement data and the model.

$$c_{\text{clean-gas}} = \frac{EDM}{w_{\text{filter}} \cdot \Delta t_{\text{cycle}}^{\gamma}} \quad (18)$$

To comply with part 1 of the study, clean-gas concentrations were calculated from the  $PM_{2.5}$  size fraction of the emitted dust mass.

$$PM_{2.5} = \frac{EDM_{PM_{2.5}}}{w_{\text{filter}} \cdot \Delta t_{\text{cycle}}^{\gamma}} \quad (19)$$

Summarizing, there is a hyperbolic behavior of the global dust emission and the cycle time in between individual filter regenerations. Introducing the “EDM” coefficient enables the prediction of particle emissions as a function of cycle time/regeneration efficiency for a certain set of parameters.

## 3 Results and Discussion

### 3.1 Validation of Experimental Data Applying the Modified Model Equations

In the consecutive sections, the experimental data from part 1 of this study is modeled applying the equations described in Sect. 2.

#### 3.1.1 Modeling of Real Differential Pressure Behavior

The differential pressure between the raw-gas side and the clean-gas side is the main result following the layout equations from Löffler [4]. Following ideal assumptions, the resistances  $K_{\text{cake}}$  and  $K_{\text{medium}}$  are sufficient to model filter operation. However, real filter behavior may deviate from the ideal assumptions (e.g., patchy cleaning, non-homogenous flow conditions, compression of the dust cake, etc.), and experimentally determined resistances under defined conditions can vary during actual filter operation [17, 18].

Hence, the medium resistance  $K_{\text{medium}}$  was varied between 10 000 and 44 000 Pa s m<sup>-1</sup> in order to determine the corresponding values for different sets of parameters. Fig. 3 shows the experimental data (connected data points) in a field of calculated differential pressure values for different filter medium resistances. At increased tank pressures, the medium resistance is lower, indicating a better filter regeneration, where the residual pressure drop is lower compared to the softer regeneration at a lower tank pressure. The concave behavior is in

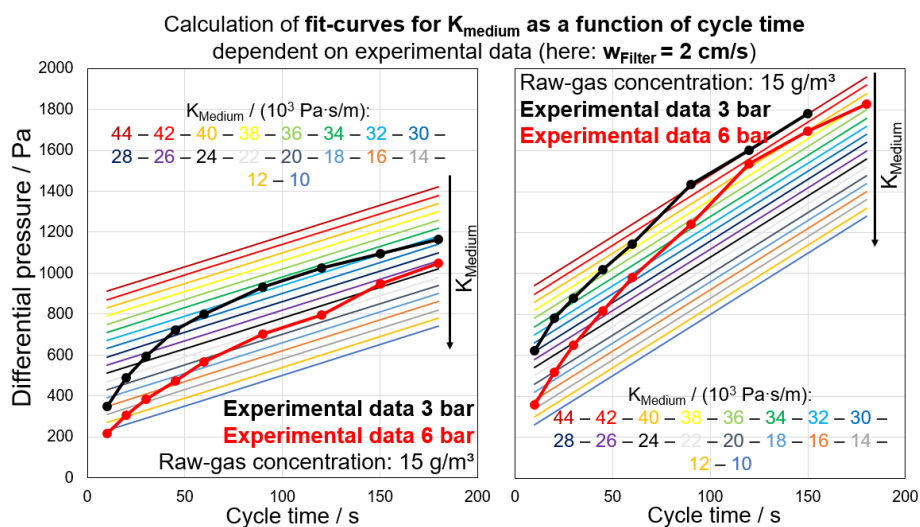


**Figure 3.** Comparison of experimental data ( $w_{\text{filter}} = 2$  cm s<sup>-1</sup>;  $p_{\text{tank}} = 3$  bar;  $c_{\text{raw-gas}} = 15$  and 30 g m<sup>-3</sup>) and model calculations varying the filter medium resistance  $K_{\text{medium}}$ .

agreement with investigations by Saleem et al. [17] who reported the differential pressure as a function of the deposited dust mass.

Out of the medium resistances, fit functions can be derived for each set of parameters to determine an empirical fit for the data. Each data point at the corresponding cycle time matches a corresponding filter medium resistance according to Fig. 3. A logarithmic fit yielded high regression coefficients for each set of experimental parameters when plotting the resistance coefficient  $K_{\text{medium}}$  as a function of the cycle time. Note that this data-driven approach enables a high agreement between model and experiment. Applying higher-degree polynomial functions would further increase the regression coefficient at the cost of a more complex set of parameters for the model. However, extrapolation would prove much more difficult due to the “arbitrary” mathematical regression within and outside of the set of experimental cycle times.

Fig. 4 shows the corresponding logarithmic fit functions and the resulting scatter plots from the calculation of  $\Delta p$  values for the experimental parameters at  $2 \text{ cm s}^{-1}$  filter face velocity. The

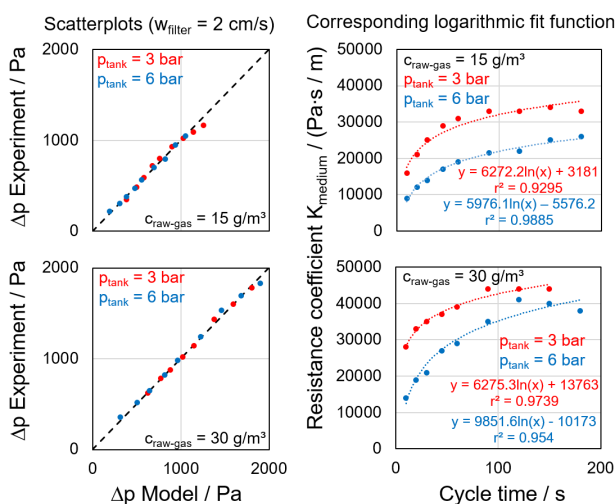


**Figure 4.** Scatter plots and corresponding logarithmic fit function for the dataset at  $2 \text{ cm s}^{-1}$  (fit functions for the rest of the dataset can be found in the Supporting Information).

logarithmic cycle time-dependent fit functions accurately predict the experimental data. Due to the large amount of available data, the calculation of the differential pressure behavior is possible for a wide range of parameters. The regression coefficients are sufficiently high (lowest  $r^2$  of 0.8823) and the remaining fit functions for each set of parameters can be found in the Supporting Information.

Due to the data-driven approach when determining the fit functions, very high correlations between experiment and model can be achieved, as expected. Of course, the optimized fit of the experimental framework comes at the trade-off of limited general accuracy outside of the experimental framework. However, the tight-knit experimental framework still enables interpolation and not only modeling of experimentally captured sets of parameters. Examples can be found in the Supporting Information.

### 3.1.2 Modeling of the Required Power for Filter Operation

After the determination of the differential pressure for each set of parameters (compare Fig. 4), the required power for filter operation can be calculated following Eqs. (9)–(11). Taking into account the required power for filter regeneration  $P_{\text{reg}}$  as presented in part 1 of this study, the total power can be determined. Fig. 5 displays the calculation of the total power and the identification of the power minimum for one set of example parameters ( $w_{\text{filter}} = 2 \text{ cm s}^{-1}$ ;  $p_{\text{tank}} = 3 \text{ bar}$ ;  $C_{\text{raw-gas}} = 15$  and  $30 \text{ g m}^{-3}$ ). The calculation results for the missing parameters (compare the full parameter set in Fig. 4) can be found in the Supporting Information.

Since the energy consumption due to filter regeneration is taken directly from experimental data, the error made from the calculation of the differential pressure is significantly lower at shorter cycle times, where the total power requirement is dominated by the contribution of filter regeneration. The identification of the broad region of the power minimum is accurately represented by the model calculations where the benefit of a higher temporal resolution of the model equations enables the exact quantification of the corresponding cycle time at minimum power. The experimental data covers relevant operation

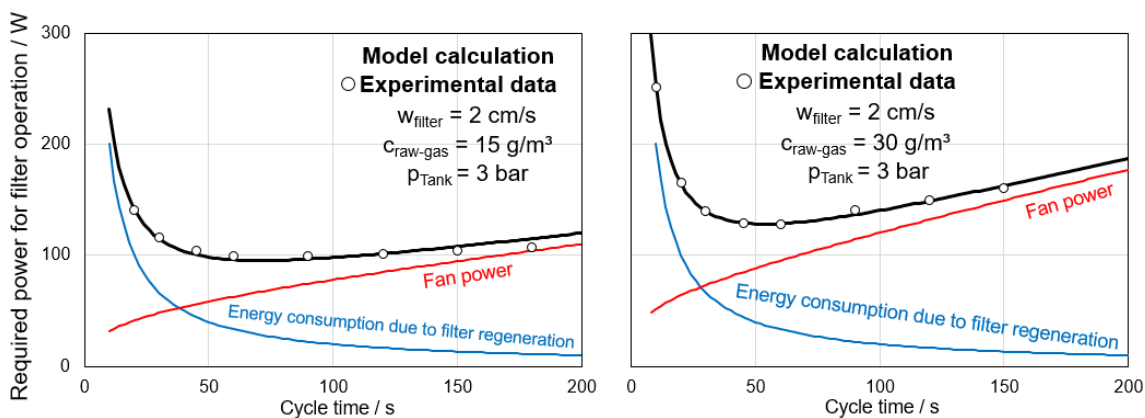


**Figure 5.** Comparison of experimental data ( $w_{\text{filter}} = 2 \text{ cm s}^{-1}$ ;  $p_{\text{tank}} = 3 \text{ bar}$ ;  $C_{\text{raw-gas}} = 15$  and  $30 \text{ g m}^{-3}$ ) and model calculations regarding the required power for filter operation.

regions ranging from shorter cycle times up to exceedingly long cycle times. The results are in qualitative agreement with the economic optimization performed by Klein et al. [19]. Extrapolation outside of the range of experimentally tested cycle times has to be handled with caution, but the logarithmic fit functions for  $K_{\text{medium}}$  at least yield plausible values as the contribution of filter regeneration to the total power.

### 3.1.3 Modeling of Particle Emissions

The particle emission is mainly independent of the cycle time and mostly dependent on other process conditions. Note that the experimental dataset offers data based on a single filter medium (at a single stage of filter life) with a single test dust and is not universally applicable. The greatest impact of particle emissions in this study is the tank pressure for filter regeneration (3 bar vs. 6 bar). For the calculation of particle emissions, the average emitted dust mass of the  $PM_{2.5}$  fraction was determined from the slopes of the individual curves shown in Fig. 2 for a tank pressure of 3 bar. Afterwards, empirical coefficients  $\gamma$  were determined based on the average  $EDM_{PM_{2.5}}$  value via minimizing the sum of absolute error between model and experiment for each set of parameters, to enable a better corre-

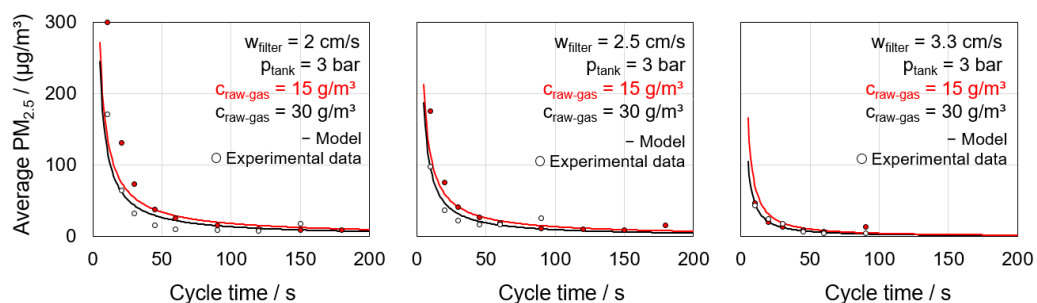
lation between experiment and model. The exact values for  $EDM_{PM_{2.5}}$  and  $\gamma$  can be found in the Supporting Information.

Fig. 6 shows a comparison between the modeled particle emissions and the experimental data for the entire set of parameters at 3 bar.

The key importance of modeling particle emissions is the overall trend in order to identify the transition point between increasingly high dust emissions and the lower emission level at higher cycle times. While particle emissions are highly dependent on many different factors (e.g., tank pressures for regeneration, filter medium, leak-free operation, filter age, etc.) and the presented emitted dust masses are not universally applicable, the hyperbolic behavior of particle emissions with increasing cycle time has to be taken into account when operating and during the layout of baghouse filters.

### 3.2 Calculation of Operation Curves

Combining the model results of Sects. 3.1.2 and 3.1.3 enables the calculation of operation curves to evaluate filter operation based on power demand and particle emissions (Fig. 7). The agreement between the experimental data and the model is sufficiently high in the region of interest around the power



**Figure 6.** Modeling of particle emissions for the entire set of experimental parameters based on the determination of the emitted dust mass ( $EDM_{PM_{2.5}}$ ) for 3 bar tank pressure and an individual empirical coefficient  $\gamma$  for each set of parameters.

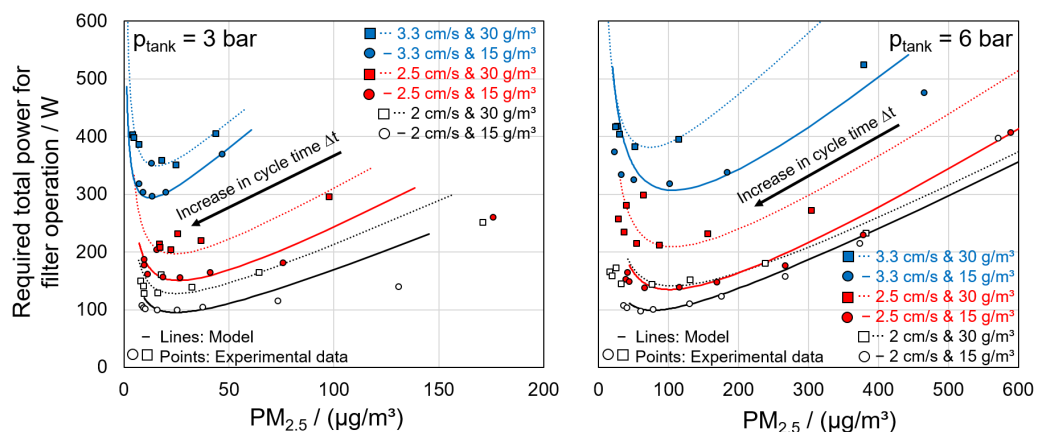


**Figure 7.** Modeled operation curves for the complete set of parameters and comparison to experimental data from part 1 of this study.

minimum. Values at either end of the experimentally tested cycle times show higher deviations.

Similarly to the experimental parameter study presented in part 1, suitable cycle times can be identified. Cycle times shorter than at the power minimum should be avoided due to increased consumption of pressurized air with no power benefit and higher particle emissions. Cycle times longer than at power minimum offer lower particle emissions at the trade-off of higher differential pressures and higher power requirements. Due to the hyperbolic behavior of particle emissions, slightly increasing the cycle time may already significantly lower the particle emissions. However, selecting increasingly long cycle times can significantly increase the power required for filter operation, with negligible effects on particle emission. Comparing the two tank pressures shows the difference in particle emissions, where the higher tank pressure requires longer cycle times to approach a zero-emission concentration.

While there are quite significant deviations and not all data points are perfectly represented by the model, especially when considering particle emissions, which were modeled semi-empirically, the overall levels calculated by the model are in good agreement. Fig. 8 shows the relevant region of (or around)

the power minimum at the corresponding cycle time  $\Delta t_{opt}$  for the experiment and the model. If no distinct power minimum could be taken from the experiments, both relevant data points are displayed.

Regarding the power for filter operation, all values are almost exactly on the same level, where the model offers an increased resolution regarding cycle times that cannot be achieved experimentally. Regarding particle emissions, the main importance is to reach a “stable emissions level” and the quantitative differences do not necessarily play a role in actual filter operation. The overwhelming trend of increased emissions with increased tank pressure is portrayed correctly, although the model does overestimate particle emissions at the power minimum.

## 4 Summary and Outlook

In part 2 of this study, the experimental data of part 1 was taken as a framework for process modeling. The transient differential behavior was modeled applying equations found in the literature [4, 15] and adapted to enable higher agreement with the experimental data. Here, the medium resistance  $K_{medium}$  was

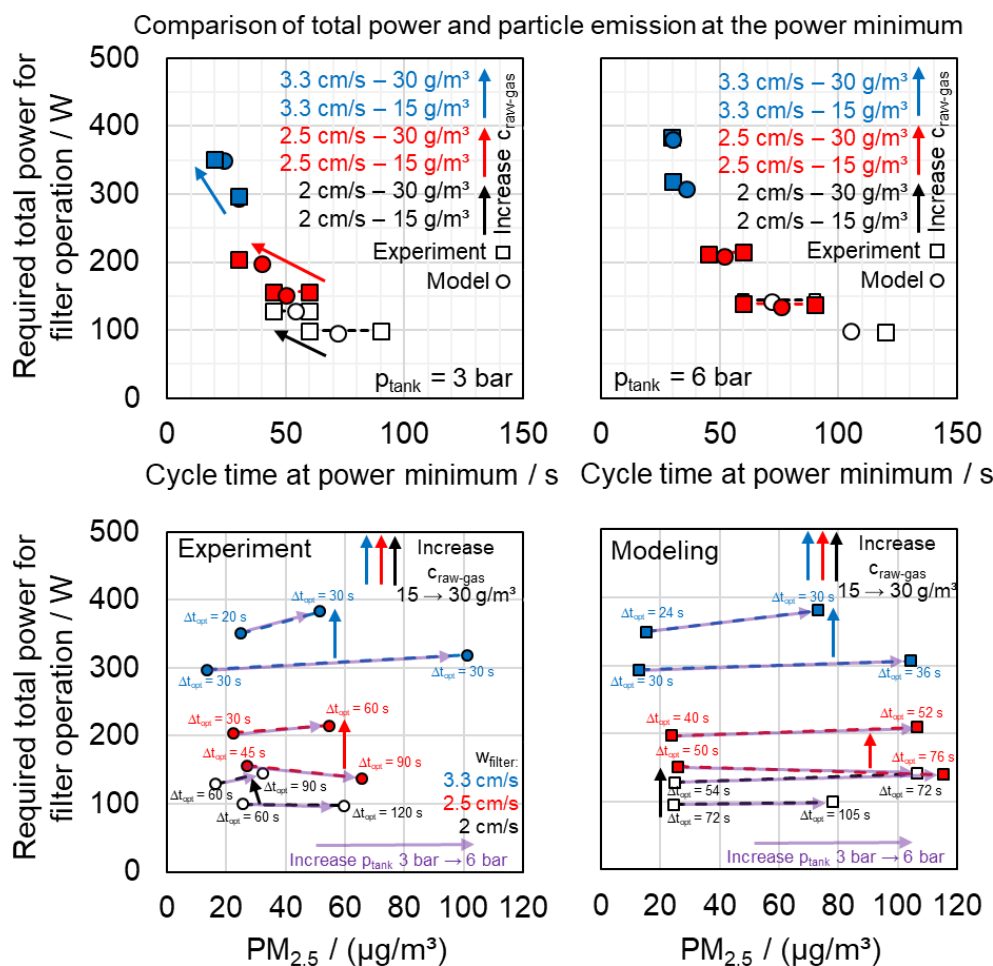


Figure 8. Comparison of model and experiment for the total power and  $\text{PM}_{2.5}$  emissions as a function of the cycle time at the power minimum for each set of parameters.



selected as flexible optimization parameter based on the cycle time, and logarithmic fit functions were derived to calculate differential pressures. The required power for filter operation was calculated as the sum of fan power and compression energy, representing the consumption of pressurized air as proposed by Höflinger and Laminger [9]. A hyperbolic dependence of particle emissions and cycle time was derived from the experimental data. Combining the energy consumption and particle emission yields operation curves at certain process parameters that enable the evaluation of filter operation and the identification of suitable operation regions. The results may help plant operators to avoid unfavorable filter operation, to improve the filter layout and shows the potential for the development of digital twins for pulse jet-cleaned filters.

## Supporting Information

Supporting Information for this article can be found under DOI: <https://doi.org/10.1002/ceat.202300409>.

## Data Availability Statement

Data available on request from the authors. The data that support the findings of this study are available from the corresponding author upon reasonable request.

## Acknowledgments

We acknowledge the financial support and close cooperation of Filterkonsortium at KIT. Filterkonsortium at KIT unites leading companies in the fields of fiber and media production, assembly, plant engineering, and measurement technology with the research activities of the research group Gas-Particle-Systems of the Institute of Mechanical Process Engineering and Mechanics (MVM). The members of Filterkonsortium at KIT are as follows: BWF Tec GmbH & Co. KG, ESTA Apparatebau GmbH & Co. KG, Freudenberg Filtration Technologies SE & Co. KG, Junker-Filter GmbH, MANN+HUMMEL GmbH, PALAS GmbH. Open access funding enabled and organized by Projekt DEAL.

*The authors have declared no conflict of interest.*

## Symbols used

$A_i$	[m <sup>2</sup> ]	filter area of a single filter element
$A_{\text{tot}}$	[m <sup>2</sup> ]	total filter area
$c_{\text{clean-gas}}$	[μg m <sup>-3</sup> ]	clean-gas concentration
$c_{\text{raw-gas}}$	[g m <sup>-3</sup> ]	raw-gas concentration
$EDM$	[μg m <sup>-2</sup> ]	total emitted dust mass per filter area
$EDM_{PM_x}$	[μg m <sup>-2</sup> ]	emitted dust mass per filter area for a certain size fraction $PM_x$
$K_i'$	[Pa s m <sup>-1</sup> ]	total resistance of a filter element

$K'_{\text{tot}}$	[Pa s m <sup>-1</sup> ]	equivalent resistance of all filter elements
$K_{\text{cake}}$	[Pa m s g <sup>-1</sup> ]	specific dust cake resistance
$K_{\text{medium}}$	[Pa s m <sup>-1</sup> ]	filter medium resistance
$n$	[-]	number of filter elements
$\Delta p$	[Pa]	differential pressure
$\Delta p_{\text{filter}}$	[Pa]	differential pressure between the raw-gas side and the clean-gas side
$p_{\text{tank}}$	[bar]	tank pressure for filter regeneration
$\Delta p_{\text{tank}}$	[Pa]	pressure drop within the pressure vessel due to filter regeneration
$P_{\text{Filter}}$	[W]	total power required for filter operation
$P_{\text{fan}}$	[W]	fan power
$P_{\text{reg}}$	[W]	energy consumption due to filter regeneration
$PM_{\text{tot}}$	[μg m <sup>-3</sup> ]	total mass concentration of particulate matter (emission)
$PM_x$	[μg m <sup>-3</sup> ]	mass concentration of a particle size fraction (e.g. $PM_{2.5}$ )
$r^2$	[-]	regression coefficient
$t$	[s]	time
$t_{\text{start}}$	[s]	starting time for integration (here: start of experiment)
$t_{\text{end}}$	[s]	end time for integration (here: end of experiment)
$\Delta t$ and $\Delta t_{\text{cycle}}$	[s]	time interval between regenerations of each individual filter element
$\Delta t_{\text{increment}}$	[s]	time increment
$\Delta t_{\text{opt}}$	[s]	time interval between regenerations at the power minimum
$\dot{V}_i$	[m <sup>3</sup> s <sup>-1</sup> ]	volume flow through a single filter element
$\dot{V}_{\text{tot}}$	[m <sup>3</sup> s <sup>-1</sup> ]	total volume flow
$V_{\text{tank}}$	[m <sup>3</sup> ]	volume of the pressure vessel for filter regeneration
$w_{\text{filter}}$	[m s <sup>-1</sup> ]	average/nominal filter face velocity
$w_{\text{filter},i}$	[m s <sup>-1</sup> ]	local filter face velocity at a single filter element
$W_i$	[g m <sup>-2</sup> ]	separated/deposited dust mass on a filter element

## Greek symbols

$\gamma$	[-]	empirical coefficient (calculation of $PM$ )
$\delta$	[-]	empirical coefficient (separation efficiency)
$\kappa$	[m <sup>2δ</sup> g <sup>-δ</sup> ]	empirical coefficient (separation efficiency)
$\eta$	[-]	separation efficiency

## References

- [1] VDI 3677 Blatt 1, Filtering Separators – Surface Filters, Beuth Verlag, Berlin 2010.
- [2] P. Bächler, J. Meyer, A. Dittler, *Chem. Eng. Technol.* **2023**, 46 (8), 1689–1697. DOI: <https://doi.org/10.1002/ceat.202300080>

- [3] O. Kurtz, J. Meyer, G. Kasper, *Chem. Eng. Technol.* **2016**, *39* (3), 435–443. DOI: <https://doi.org/10.1002/ceat.201500340>
- [4] F. Löffler, *Staubabscheiden*, Georg Thieme Verlag, Stuttgart **1988**.
- [5] X. Simon, D. Bémer, S. Chazelet, D. Thomas, R. Régnier, *Powder Technol.* **2010**, *201*, 37–48. DOI: <https://doi.org/10.1016/j.powtec.2010.02.036>
- [6] P. Bächler, J. Szabadi, J. Meyer, A. Dittler, *J. Aerosol Sci.* **2022**, *150*, 105644. DOI: <https://doi.org/10.1016/j.jaerosci.2020.105644>
- [7] DIN ISO 11057, Air quality – Test method for filtration characterization of cleanable filter media, Beuth Verlag, Berlin **2012**.
- [8] J. Binnig, J. Meyer, G. Kasper, *Powder Technol.* **2009**, *189* (1), 108–114. DOI: <https://doi.org/10.1016/j.powtec.2008.06.012>
- [9] W. Höflinger, T. Laminger, *Energy Sustainability* **2013**, *4*, 145–155. DOI: <https://doi.org/10.2495/ESUS130121>
- [10] T. Sinn, P. Menesklou, H. Nirschl, M. Gleiß, *Chem. Eng. Sci.* **2023**, *277*, 118858. DOI: <https://doi.org/10.1016/j.ces.2023.118858>
- [11] H. K. Baust, S. Hammerich, H. König, H. Nirschl, M. Gleiß, *Separations* **2022**, *9* (9), 248. DOI: <https://doi.org/10.3390/separations9090248>
- [12] F. Rhein, L. Hibbe, H. Nirschl, *Eng. Comput.* **2023**. DOI: <https://doi.org/10.1007/s00366-023-01809-8>
- [13] W. Solbach, *Staub – Reinhalt. Luft* **1969**, *1*, 24–28.
- [14] R. Dennis, H. A. Klemm, *J. Air Pollut. Control Assoc.* **1980**, *30* (1), 38–43. DOI: <https://doi.org/10.1080/00022470.1980.10465912>
- [15] D. Leith, M. J. Ellenbecker, *Atmos. Environ.* **1980**, *14* (7), 845–852. DOI: [https://doi.org/10.1016/0004-6981\(80\)90141-9](https://doi.org/10.1016/0004-6981(80)90141-9)
- [16] E. Schmidt, *Chem. Ing. Tech.* **1995**, *67* (4), 464–467. DOI: <https://doi.org/10.1002/cite.330670409>
- [17] M. Saleem, G. Krammer, M. S. Tahir, *Powder Technol.* **2012**, *228*, 100–107. DOI: <https://doi.org/10.1016/j.powtec.2012.05.003>
- [18] Z. Potok, T. Rogozinski, *Sustainability* **2020**, *12* (12), 4816. DOI: <https://doi.org/10.3390/su12124816>
- [19] G.-M. Klein, T. Schrooten, T. Neuhaus, *Chem. Ing. Tech.* **2012**, *84* (7), 1121–1129. DOI: <https://doi.org/10.1002/cite.201100251>
- [20] E. Schmidt, *Powder Technol.* **1996**, *86* (1), 113–117. DOI: [https://doi.org/10.1016/0032-5910\(95\)03044-1](https://doi.org/10.1016/0032-5910(95)03044-1)
- [21] Q. Zhang, D. Horst, E. Schmidt, *Chem. Ing. Tech.* **2020**, *92* (3), 275–281. DOI: <https://doi.org/10.1002/cite.201900116>
- [22] Q. Zhang, *Chem. Ing. Tech.* **2022**, *94* (4), 572–584. DOI: <https://doi.org/10.1002/cite.202100053>
- [23] U. Heck, M. Becker, CFD modelling of a bag filter plant for flue gas cleaning under consideration of flow shift and particle deposition relocations, presented at *Filtech – the Filtration Event*, Cologne **2022**.
- [24] E. Schmidt, *Abscheidung von Partikeln aus Gasen mit Oberflächenfiltern*, Fortschritt-Berichte der VDI-Zeitschriften, Reihe 3, 546, VDI Verlag, Düsseldorf **1998**.
- [25] E. Schmidt, Dust separation, in *Ullmann's Encyclopedia of Industrial Chemistry*, Wiley-VCH, Weinheim **2023**. DOI: [https://doi.org/10.1002/14356007.b02\\_13.pub3](https://doi.org/10.1002/14356007.b02_13.pub3)
- [26] European Commission, Joint Research Centre, K. Daginnus, T. Marty, N. Valeria Trotta, et al., *Best available techniques (BAT) reference document for common waste gas management and treatment systems in the chemical sector: Industrial Emissions Directive 2010/75/EU (integrated pollution prevention and control)*, Publications Office of the European Union, Luxembourg **2023**. <https://data.europa.eu/doi/10.2760/220326>
- [27] A. Dittler, M. V. Ferer, P. Mathur, P. Djuranovic, G. Kasper, D. H. Smith, *Powder Technol.* **2002**, *124* (1/2), 55–66. DOI: [https://doi.org/10.1016/S0032-5910\(01\)00481-8](https://doi.org/10.1016/S0032-5910(01)00481-8)
- [28] P. Bächler, J. Meyer, A. Dittler, *Gefahrstoffe – Reinhalt. Luft* **2019**, *79* (11/12), 433–450. DOI: <https://doi.org/10.37544/0949-8036-2019-11-12-49>

**Research Article:** The operating behaviour of a pulse jet-cleaned filter is calculated applying and adapting model equations, demonstrating the trade-off between energy demand and particle emissions.

## Operating Behavior of Pulse Jet-Cleaned Filters Regarding Energy Demand and Particle Emissions – Part 2: Modeling

Peter Bächler\*, Jörg Meyer,  
Achim Dittler

*Chem. Eng. Technol.* 2024, 47 (XX),  
XXX ... XXX

DOI: 10.1002/ceat.202300409



Supporting Information  
available online

